First-principles study on the electronic, optical, and transport properties of monolayer α- and β-GeSe

Yuanfeng Xu,[1] Hao Zhang,[1,2,3,*] Hezhu Shao,[4] Gang Ni,[1] Jing Li,[1] Hongliang Lu,[5] Rongjun Zhang,[1] Bo Peng,[1] Yongyuan Zhu,[2] Heyuan Zhu,[1,†] and Costas M. Soukoulis[3,6]

[1]*Department of Optical Science and Engineering and Key Laboratory of Micro and Nano Photonic Structures (Ministry of Education), Fudan University, Shanghai 200433, China*

[2]*National Laboratory of Solid State Microstructure, Nanjing University, Nanjing 210093, China*

[3]*Department of Physics and Astronomy and Ames Laboratory, Iowa State University, Ames, Iowa 50011, USA*

[4]*Ningbo Institute of Materials Technology and Engineering, Chinese Academy of Sciences, Ningbo 315201, China*

[5]*State Key Laboratory of ASIC and System, Institute of Advanced Nanodevices, School of Microelectronics, Fudan University, Shanghai 200433, China*

[6]*Institute of Electronic Structure and Laser, FORTH, 71110 Heraklion, Crete, Greece*

(Received 29 August 2017; revised manuscript received 29 November 2017; published 22 December 2017)

The extraordinary properties and the novel applications of black phosphorene induce the research interest in the monolayer group-IV monochalcogenides. Here using first-principles calculations, we systematically investigate the electronic, transport, and optical properties of monolayer α- and β-GeSe, revealing a direct band gap of 1.61 eV for monolayer α-GeSe and an indirect band gap of 2.47 eV for monolayer β-GeSe. For monolayer β-GeSe, the electronic/hole transport is anisotropic, with an extremely high electron mobility of 2.93×10^4 cm^2/V s along the armchair direction, comparable to that of black phosphorene. Furthermore, for β-GeSe, robust band gaps nearly independent of the applied tensile strain along the armchair direction are observed. Both monolayer α- and β-GeSe exhibit anisotropic optical absorption in the visible spectrum.

DOI: 10.1103/PhysRevB.96.245421

I. INTRODUCTION

The atomic-monolayer materials, also called two-dimensional (2D) materials, have received tremendous attentions since the experimental realization of graphene [1–3]. Nowadays, 2D materials have formed a large material family, involving various kinds of layered crystal structures and chemical elements, e.g., graphene [4–6], transition-metal dichalcogenides [7–10], stanene [11,12], penta-graphene [13,14], etc.

Recently, black phosphorene, a monolayer material composed of phosphorus atoms with a puckered structure, has attracted much attention because of its extraordinary properties. Black phosphorene is a semiconductor with a direct band gap of 1.5 eV [15,16], and it has a strongly anisotropic transport property with a high hole mobility comparable to that of graphene [16–19], which makes it a promising candidate for future electronic and optoeletronic applications. Many efforts have been devoted to the discovery of new 2D materials with "phosphorene-analog" puckered structure [20] since the successful prediction of black phosphorene. Following the prediction approach called the "atomic transmutation" method [21], in which one type of element is changed (transmuted) into its neighboring elements in the periodic table but the total number of valence electrons is kept unchanged, the monolayer of group-IV monochalcogenides MX (M = Ge, Sn; X = S, Se) with similar puckered structures is believed to possess properties similar to those of black phosphorene and can be regarded as a family of phosphorene analog [20,22–24].

The properties of the material family MX in the bulk form have been intensely investigated, and these materials have been revealed to be excellent thermoelectric materials with a high figure of merit [25], especially for the crystal SnSe, which has an extraordinarily high thermoelectric ZT value of 2.6 ± 0.3 at 923 K [26]. Much attention has been devoted to studying electronic and optical properties [20,22], piezoelectricity [23,24], and thermoelectric and phonon transport [25] properties of monolayer MX. Recently, Rohr *et al.* predicted a new member of the MX family, i.e., β-GeSe, which is a polymorph of GeSe [27] with a boat conformation for its Ge-Se six-membered ring. Experimental measurement and theoretical calculations reveal that monolayer β-GeSe, similar to another polymorph of GeSe, i.e., α-GeSe [28], is a semiconductor with a moderate band gap as well, which makes it promising for future electronic and optoelectronic applications. Further investigations of monolayer β-GeSe and some related monolayer MX crystals are thus necessary to gain insights into this new kind of 2D material.

In this work, we systematically investigate the electronic, transport, and optical properties of monolayer α- and β-GeSe by using first-principles calculations. We demonstrate that the direct band gap of monolayer α-GeSe is smaller than the indirect band gap of β-GeSe. Monolayers of both α- and β- GeSe have exceptionally high electron mobilities, which are predicted to be 4.71×10^3 and 2.93×10^4 cm^2/V s, respectively, with strong anisotropy. Furthermore, we also investigate the strain-engineering and optical properties of these two materials.

II. METHOD AND COMPUTATIONAL DETAILS

The calculations are performed using the Vienna Ab initio Simulation Package (VASP) based on density functional theory (DFT) [29]. The exchange-correlation energy is described by the generalized gradient approximation using the Perdew-

*zhangh@fudan.edu.cn
†hyzhu@fudan.edu.cn

Burke-Ernzerhof (PBE) functional. The calculation is carried out by using the projector augmented-wave pseudopotential method with a plane-wave basis set with a kinetic-energy cutoff of 600 eV. Furthermore, for Ge and Se atoms, we considered d and p semicore states, respectively, as valence states by choosing Ge_d and Se pseudopotentials. When optimizing atomic positions, the energy convergence value between two consecutive steps is chosen to be 10^{-5} eV, and the maximum Hellmann-Feynman (HF) force acting on each atom is 10^{-3} eV/Å. For an α-GeSe monolayer, the Monkhorst-Pack scheme is used for the Brillouin zone integration with k-point meshes of $17 \times 15 \times 1$ and $25 \times 21 \times 1$ for geometry optimization and self-consistent electronic structure calculations, respectively. For the β phase, we use $17 \times 11 \times 1$ and $25 \times 15 \times 1$ Monkhorst-Pack k meshes for the structure relaxation and electronic structure calculations, respectively. To verify the results of the PBE calculations, the electronic structures of α- and β-GeSe are calculated using the much more computationally expensive hybrid Heyd-Scuseria-Ernzerhof (HSE06) functional [30]. Generally, HSE06 improves the precision of the band gap by reducing the localization and delocalization errors of PBE and HF functionals. Herein, the screening parameter u is set to 0.2 Å^{-1}. The complex dielectric functions $\epsilon(\omega)$ of monolayer α- and β-GeSe are calculated by using the HSE06 hybrid functional on a grid of $11 \times 11 \times 1$. The tetrahedron method with Blöchl corrections is used as the smearing scheme. The effect of the van der Waals interactions between adjacent layers was considered by using the empirical correction scheme of Grimme's DFT-D2 (PBE-D2) method [31,32].

The properties of monolayer α- and β-GeSe are obtained based on the results of a complex dielectric function, i.e., $\epsilon(\omega) = \epsilon_1(\omega) + i\epsilon_2(\omega)$. The imaginary part of the dielectric tensor $\epsilon_2(\omega)$ is determined by a summation over empty band states as follows [33]:

$$\epsilon_2(\omega) = \frac{2\pi e^2}{\Omega\epsilon_0} \sum_{k,v,c} \delta\left(E_k^c - E_k^v - \hbar\omega\right) \left|\left\langle \Psi_k^c \middle| \mathbf{u}\cdot\mathbf{r} \middle| \Psi_k^v \right\rangle\right|^2, \quad (1)$$

where ϵ_0 is the vacuum dielectric constant, Ω is the crystal volume, v and c represent the valence and conduction bands, respectively, $\hbar\omega$ is the energy of the incident photon, $\mathbf{u}$ is the vector defining the polarization of the incident electric field, $\mathbf{u}\cdot\mathbf{r}$ is the momentum operator, Ψ_k^c and Ψ_k^v are the wave functions of the conduction and valence bands at the k point, respectively. The real part of the dielectric tensor $\epsilon_1(\omega)$ is obtained with the well-known Kramers-Kronig relation [34],

$$\epsilon_1(\omega) = 1 + \frac{2}{\pi} P \int_0^\infty \frac{\epsilon_2(\omega')\omega'}{\omega'^2 - \omega^2 + i\eta} d\omega', \quad (2)$$

where P denotes the principle value. The absorption coefficient $\alpha(\omega)$ and reflectivity $R(\omega)$ can be subsequently given by [35–37]

$$\alpha(\omega) = \frac{\sqrt{2}\omega}{c} \left\{ \left[\epsilon_1^2(\omega) + \epsilon_2^2(\omega)\right]^{1/2} - \epsilon_1(\omega) \right\}^{\frac{1}{2}}, \quad (3)$$

$$R(\omega) = \left| \frac{\sqrt{\epsilon_1(\omega) + i\epsilon_2(\omega)} - 1}{\sqrt{\epsilon_1(\omega) + i\epsilon_2(\omega)} + 1} \right|^2. \quad (4)$$

By using the deformation potential theory for semiconductors, which was proposed by Bardeen and Shockley [38], the intrinsic carrier mobility μ of monolayer group-IV monochalcogenides (α-GeS, α-GeSe, α-SnS, α-SnSe, and β-GeSe) is calculated and investigated in detail herein. In the long-wavelength limit, when considering only the interaction between the electron and longitudinal acoustic phonon [38,39], the carrier mobility of 2D semiconductors is given by [40–43]

$$\mu = \frac{e\hbar^3 C^{2D}}{k_B T m_e^* m_d E_l^2}, \quad (5)$$

where e is the electron charge, $\hbar$ is the reduced Planck's constant, and T is the temperature, equal to 300 K throughout the paper. C^{2D} is the elastic modulus of a crystal uniformly deformed by strains and derived from $C^{2D} = [\partial^2 E/\partial^2(\Delta l/l_0)]/S_0$, in which E is the total energy, Δl is the change in the lattice constant l_0 along the transport direction, and S_0 represents the lattice volume at equilibrium for a 2D system; m_e^* is the effective mass along the transport direction, given by $m_e^* = \hbar^2[\partial^2 E(k)/\partial k^2]^{-1}$ [k is the wave vector, and $E(k)$ denotes the energy; either m_a^* or m_b^* along the a or b direction, respectively], and m_d is the average effective mass, defined by $m_d = \sqrt{m_a^* m_b^*}$. E_l is the deformation potential (DP) constant, defined by $E_l^{e(h)} = \Delta E_{\mathrm{CBM(VBM)}}/(\Delta l/l_0)$, where $\Delta E_{\mathrm{CBM(VBM)}}$ is the energy shift of the band edge with respect to the vacuum level under a small dilation Δl of the lattice constant l_0.

III. RESULTS AND DISCUSSION

A. Geometric structure of monolayer α- and β-GeSe

The top and side views of the fully optimized structure of monolayer α- and β-GeSe, both with space group $Pmn2_1(31)$, are shown in Figs. 1(a)–1(d), respectively. Both monolayer α- and β-GeSe consist of two atomic sublayers. The α- and β-GeSe monolayers are optimized with vacuum layers of 21 and 16 Å, respectively, which are large enough to

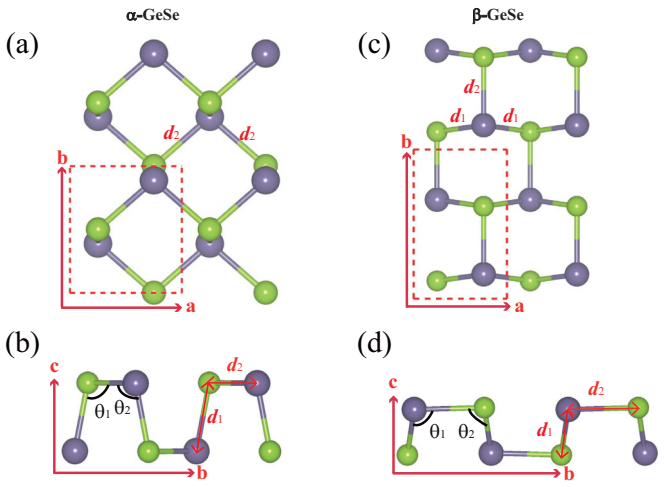

FIG. 1. Atomic structure of monolayer α- and β-GeSe in a $2 \times 2 \times 1$ supercell from (a) and (c) the top view and (b) and (d) side view, respectively. The a (b) direction is the zigzag (armchair) direction. The blue and green balls denote Ge and Se atoms, respectively.

avoid the artificial interaction between atom layers. The tetragonal unit cell (the dashed rectangle) of monolayer α- and β-GeSe contains two germanium atoms and two selenium atoms. From the top view and side view of α-GeSe, as shown in Figs. 1(a) and 1(b), monolayer α-GeSe is a puckered-structure analog to black phosphorene with Ge and Se atoms substituted for P atoms alternately [15,44,45]. Similar monolayer structures can be found in monolayer black phosphorene and other group-IV monochalcogenides MX (M = Ge or Sn; X = S or Se), e.g., α-GeS, α-GeSe, α-SnS, and α-SnSe, as shown in the Supplemental Material [46].

Monolayer β-GeSe, which consists of six rings with the vertices arranged in an uncommon boat conformation [27], as shown in Figs. 1(c) and 1(d), can be mechanically exfoliated from the bulk phase due to the weak van der Waals bonding between adjacent monolayers, and the Supplemental Material [46] shows the structures of bulk and monolayer β-GeSe from the top and side views.

Based on the first-principles method, the lattice constants of α-GeSe are calculated to be $a = 3.97$ Å and $b = 4.29$ Å, which are in good agreement with reported experimental ($a = 3.83$ Å and $b = 4.39$ Å) [27] and theoretical ($a = 3.96$ Å and $b = 4.16$ Å in Ref. [47], $a = 3.93$ Å and $b = 4.27$ Å in Ref. [24], and $a = 3.90$ Å and $b = 4.24$ Å in Ref. [48]) results. Each Ge/Se atom binds three neighboring Se/Ge atoms with different bond lengths, as shown in Figs. 1(a) and 1(b), and two of them are identical, with $d_2 = 2.66$ Å, and the other one is $d_1 = 2.54$ Å. The bond angles of $\theta_{\mathrm{Ge-Se-Ge}}$ and $\theta_{\mathrm{Se-Ge-Se}}$ are 96.59° and 97.41°, respectively. For monolayer β-GeSe, the optimized lattice constants are $a = 3.67$ Å and $b = 5.91$ Å, which are in good agreement with experimental results ($a = 3.83$ Å and $b = 5.81$ Å) [27]. In this boat structure of β-GeSe, each Ge atom binds three Se atoms with two identical bond lengths of $d_1 = 2.55$ Å and one bond length of $d_2 = 2.72$ Å, and the bond angles of $\theta_{\mathrm{Ge-Se-Ge}}$ and $\theta_{\mathrm{Se-Ge-Se}}$ are 93.91° and 96.65°, respectively. For comparison, the calculated lattice parameters, bond lengths, and bond angles for black phosphorene and other α-structures of group-IV monochalcogenides MX are shown in Table S1.

For monolayer α-GeSe, shown in Fig. 2(a), both the conduction-band minimum (CBM) and the valence-band maximum (VBM) are located along the Γ-Y direction, denoted by C_y and V_y, respectively. The formation of the band gap of α-GeSe shows that it is a semiconductor with a direct band gap of 1.16 eV, which is well consistent with the reported results (1.16 eV in Refs. [25,47], 1.22 eV in Ref. [49]) [25,47,49]. However, it is worth mentioning that the energy difference (0.014 eV) between the local CBMs [C_X and C_Y in Fig. 2(a)] and the CBM at k_{CBM} is very small, and such nearly degenerate CBMs suggest that it is feasible to apply some kind of external controls (e.g., strain) to tune monolayer α-GeSe from direct to indirect semiconductors or vice versa. Since Ge and Se are relatively heavy elements, the spin-orbit-coupling (SOC) effect may influence the band structures obviously, which is confirmed by the calculated band structures with SOC involved, as shown in Fig. 2(a) (the red dashed line). The corresponding HSE06 calculation without SOC (with SOC)

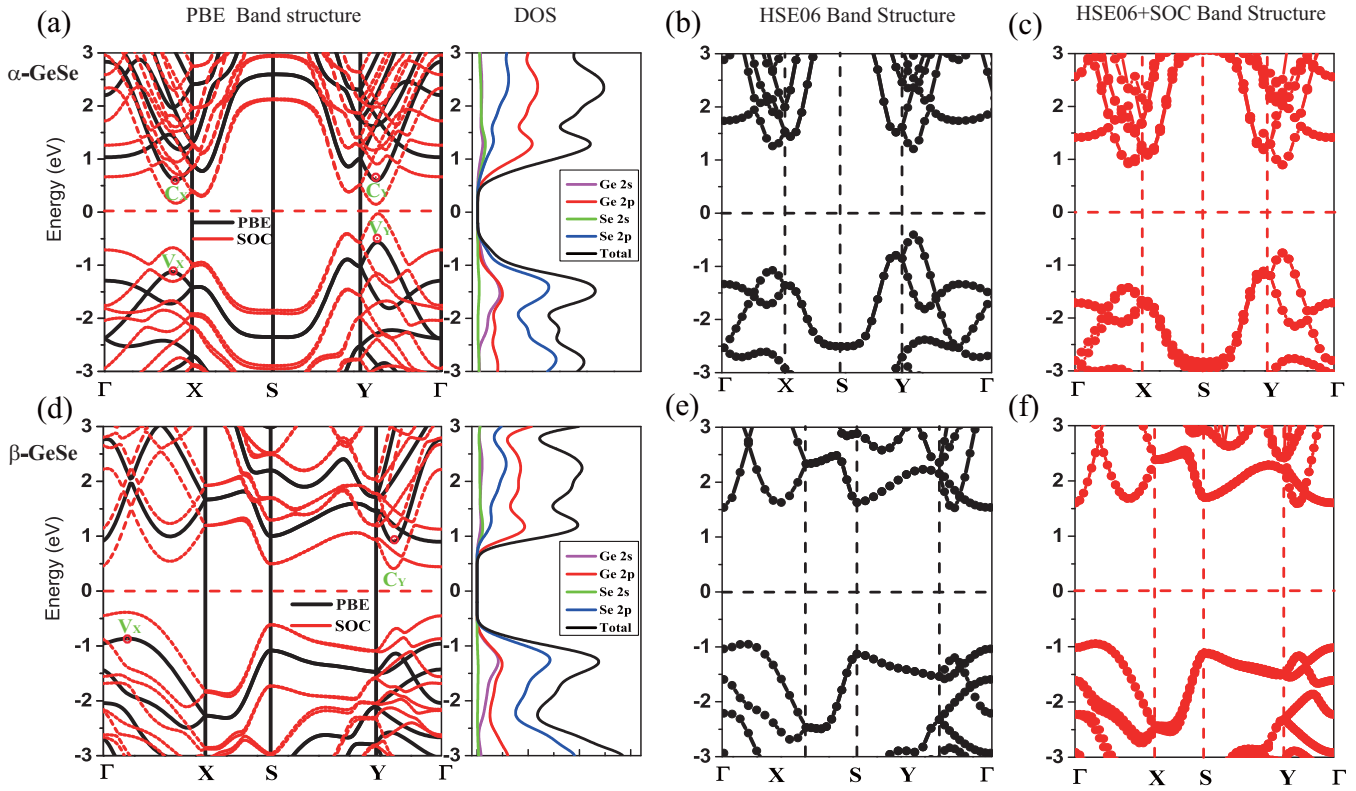

FIG. 2. (a) and (d) PBE calculations with and without SOC of the electronic band structure and PBE calculated density of states (DOS) of monolayer α-GeSe and β-GeSe along high-symmetry directions, respectively. (b) and (e) Electronic band structures under the HSE06 hybrid functional of monolayer α-GeSe and β-GeSe, respectively. (c) and (f) HSE06 band calculations with SOC.

in Fig. 2(b) [Fig. 2(c)] gives a larger band gap of 1.61 eV (1.67 eV) compared to the PBE result of 1.16 eV since PBE calculations always underestimate the value of band gaps of semiconductors.

As mentioned above, the α-structure of group-IV monochalcogenides MX can be regarded as the results of material design by atomic transmutation from monolayer black phosphorene, in which the P atoms are changed by a group-IV atom (Ge/Sn) and a group-VI atom (S/Se) and the total number of valence electrons is kept unchanged. Therefore, the similarity of the electronic band structures between monolayer black phosphorene and α-MX is expected (results shown in the Supplemental Material [46]), resulting from the structural similarity and the similar p-orbital electrons contributions. By comparison with the band gaps of black phosphorene and other monolayer α-MX under investigations here (see the Supplemental Material [46]) it is found that only black phosphorene and α-GeSe possess direct band gaps, while the other phosphorene analogs, including β-GeSe, possess indirect band gaps, which means that only monolayer black phosphorene and α-GeSe possess a good ability to absorb photons, while the photon-absorption abilities of β-GeSe and other α-MX are relatively poor since photons are necessarily involved.

The PBE calculations with and without SOC for the electronic band structure and DOS of monolayer β-GeSe are presented in Fig. 2(d), which shows that monolayer β-GeSe is a semiconductor with an indirect band gap with E_g = 1.76 eV. The CBM locates at the midpoint along the Γ-Y direction, and the VBM locates near the Γ point along the Γ-X direction. The obtained band gap decreases to 0.80 eV when the SOC is involved. The HSE06 calculations with and without SOC effects for β-GeSe give band gaps of 2.53 and 2.47 eV, respectively, which are larger than that of α-GeSe.

As for the SOC effects, since the calculated SOC strength is negative, as shown in Table I, the calculated band gaps for both α- and β-GeSe decrease when SOC is involved.

In order to clarify the contributions from different orbitals to the band structures around the Fermi level of α- and β-GeSe, we calculate the total and partial densities of states (DOSs), as shown in the right part of Figs. 2(a) and 2(e). Analysis of the partial DOS (PDOS; Ge 4s, 4p and Se 4s, 4p orbitals) of α-GeSe reveals that Ge 4p and Se 4p orbitals dominate the electronic states near the Fermi level. The contributions from the Ge 4p orbitals to the total DOS of the conduction bands is larger than that from Se 4p, while in the valence band, the Se 4p orbitals have greater contributions than those from Ge 4p. Analysis of the PDOS of monolayer β-GeSe reveals the dominant contributions from Ge 4p and Se 4p orbitals to the total DOS near the Fermi level, and the respective contribution from the Ge 4p and Se 4p orbitals is similar to the case of α-GeSe. A similar analysis of the PDOS on other α-MX also leads to the result that the p orbital of group-IV (group-VI) atoms dominates the conduction (valence) bands. It worth noting that, to correct the underestimation of the band gap of standard DFT calculations, the DFT + U approach can be used by setting the on-site Coulomb parameter U and J to Ge atoms.

B. Electronic band structure of 2D α- and β-GeSe

The calculated electronic band structures performed by both PBE (with and without SOC) and the HSE06 hybrid functional method for monolayer α- and β-GeSe along high-symmetry directions of the Brillouin zone are shown in Fig. 2. The above-mentioned PDOS analysis of the orbital contributions to the formation of CBM and VBM is validated by the partial charge densities associated with the CBM and VBM for both monolayer α- and β-GeSe, as shown in Fig. 3. In both materials, the p orbitals of Ge atoms contribute dominantly to CBM by connecting the neighboring Se atoms via antibonding states, as shown in Figs. 3(a) and 3(b) and 3(e) and 3(f); however, VBM is dominated by the contribution from p orbitals of Se atoms by connecting the neighboring Ge atoms via bonding states, as shown in Figs. 3(c) and 3(d) and 3(g) and 3(h).

C. Strain-engineering electronic properties of monolayer α- and β-GeSe

Here we study the effects of in-plane uniaxial (a and b direction) and biaxial (bi: **a** + **b** directions) strains on electronic properties of monolayer α- and β-GeSe to realize the possible tunability of their electronic properties [50]. In this work, ε_x, ε_y, and ε_{xy} indicate the components of the relative strain along the a, b, and bi directions, respectively. The positive (negative) values represent tensile (compressive) strain and are evaluated as the lattice stretching (condensing) percentage. All the applied strains here are in the elastic region [51], which is confirmed by the quadratic dependence of strained energy on the applied strains (see the Supplemental Material [46]).

Figure 4 shows the valence- and conduction-band structures of monolayer α-GeSe as a function of different strains, from -10% to 10% of the fully relaxed structure. Figures 4(a)–4(c) show the dependence of the energy bands on strain along the a, b, and bi directions, respectively. Figure 4(d) shows the evolution of calculated band gap under various strains.

The VBMs (V_X and V_Y) and CBMs (C_X and C_Y) are shown in Fig. 4. Monolayer α-GeSe without strains is a direct semiconductor described by VBM V_Y and CBM C_Y. When compressive strains are applied along the a direction, the values of V_Y and C_Y increase, while the value of C_X decreases, leading to a transition from the direct to indirect semiconductor

TABLE I. Structural information, cohesive energies E_c, SOC strength E^{SOC}, and band gaps of monolayer α- and β-GeSe. E_g(PBE(SOC)/HSE06(SOC)) is the value of band gap calculated using PBE (HSE06) functionals without and with SOC, respectively. The bond angles θ and bond lengths d are indicated in Fig. 1.

Phase	a	b	d_1	d_2 (Å)	θ_1	θ_2 (deg)	E_c (eV/atom)	E^{SOC}_{Ge}	E^{SOC}_{Se} (eV)	E_g(PBE(SOC)/HSE06(SOC)) (eV)
α	3.97 (3.83 [27])	4.29 (4.39 [27])	2.54	2.66	96.59	97.41	−4.20	−0.016	−0.040	1.16 (0.18)/1.61 (1.67)
β	3.67 (3.83 [27])	5.91 (5.81 [27])	2.55	2.72	96.65	93.91	−4.17	−0.016	−0.041	1.76 (0.80)/2.47 (2.53)

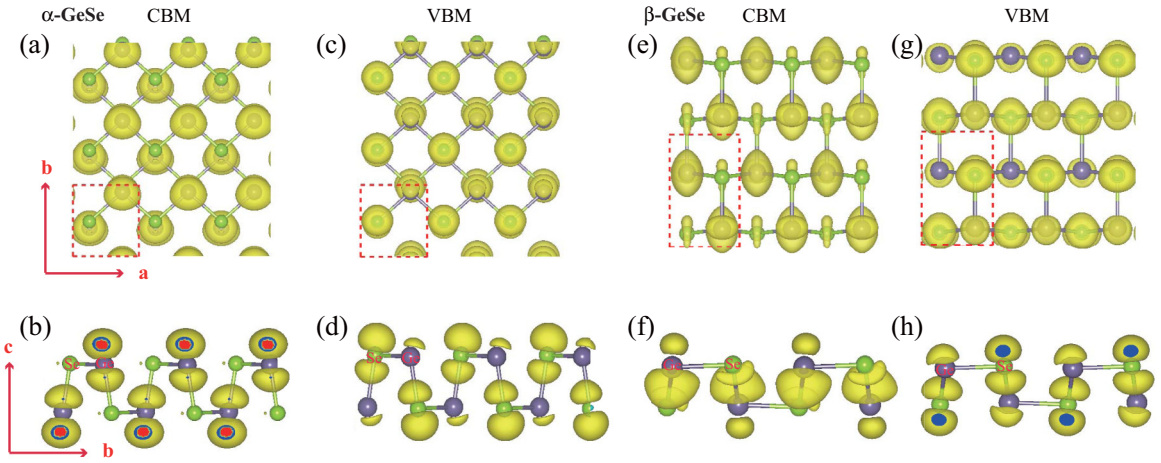

FIG. 3. Isosurface plots of the charge density of (a) and (b) CBM and (c) and (d) VBM for monolayer α-GeSe and (e) and (f) CBM and (g) and (h) VBM for monolayer β-GeSe illustrated in the ab and bc planes, with an isovalue of 0.007 $e/\text{Å}^3$.

of monolayer α-GeSe even at a small compression with $\varepsilon_x = -1\%$. When a compressive strain of $\varepsilon_x = -8\%$ is applied, a semiconductor-to-metal transition takes place, as shown in Fig. 4(d).

However, when applying a tensile strain along the a direction, the changes in the local VBM and CBM are different. When the tensile strain increases, the value of local V_Y decreases, and the values of C_X and V_X increase, while the value of C_Y remains nearly unchanged, subsequently leading to a transition from direct to indirect semiconductors at $\varepsilon_x = 9\%$. So the direct band gap characteristic of monolayer α-GeSe remains unchanged for small compression and moderate stretching along the a direction (from $\varepsilon_x = -1\%$ to $\varepsilon_x = 9\%$).

The change in the band structures of monolayer α-GeSe when applying an external strain along the b direction (ε_y) is much smaller than that for strains along the a direction;

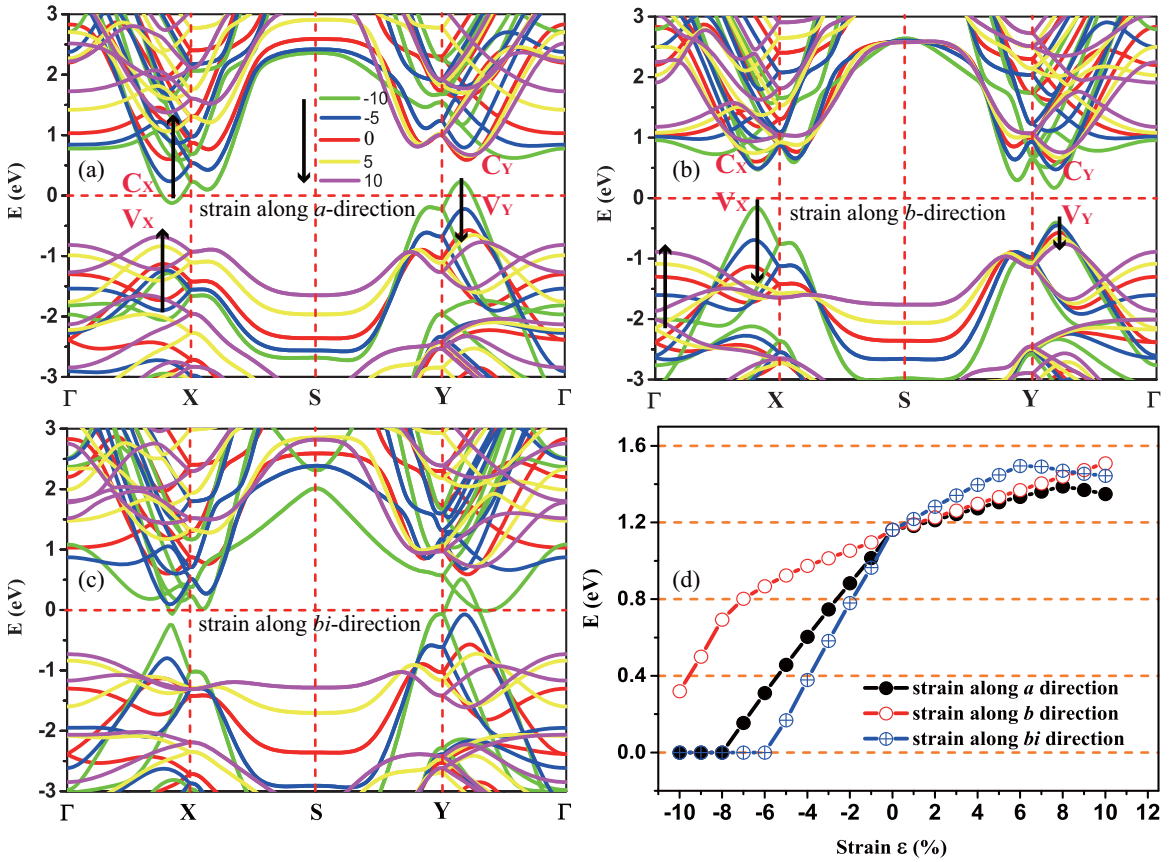

FIG. 4. Electronic band structures of monolayer α-GeSe under applied strains along (a) the a direction, (b) the b direction, and (c) the bi direction. (d) The evolution of band gaps for α-GeSe as a function of the applied strain.

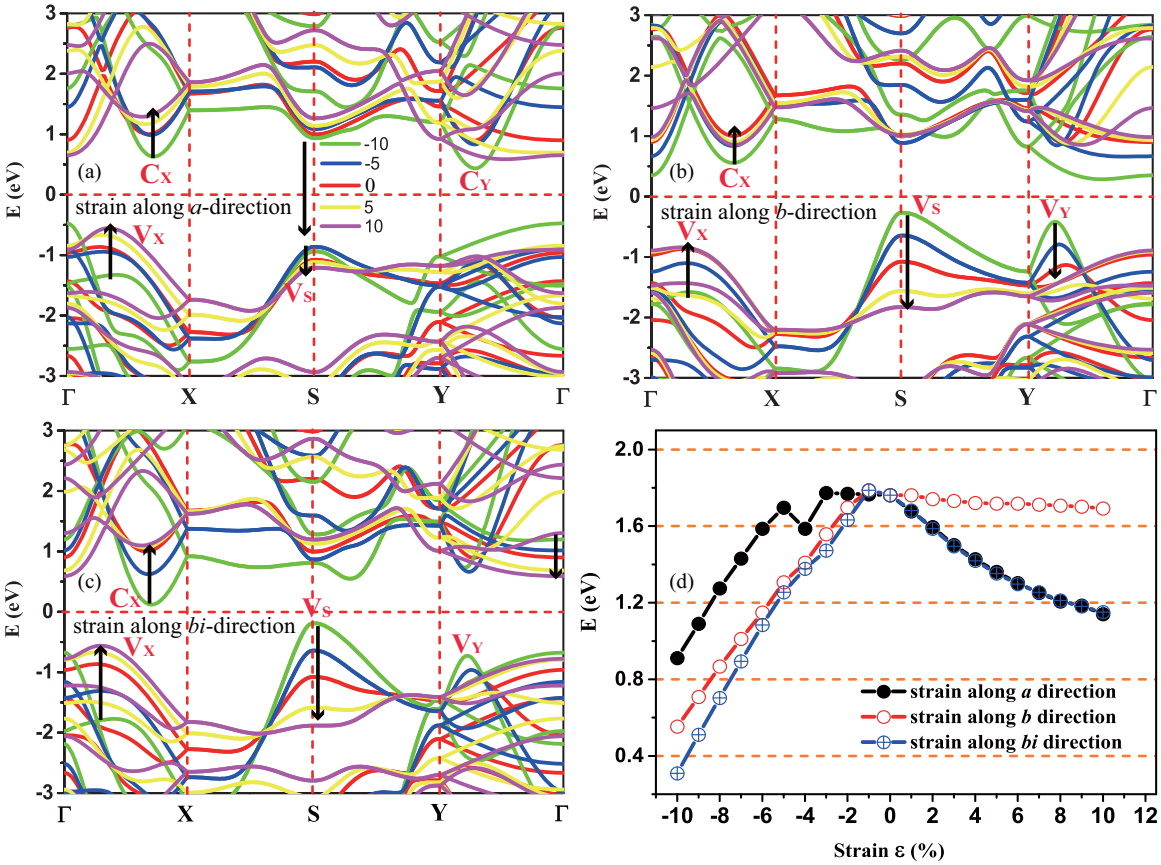

FIG. 5. Electronic band structures of monolayer β-GeSe under applied strains along (a) the a direction, (b) the b direction, and (c) the bi direction. (d) The evolution of band gaps for β-GeSe as a function of the applied strain.

a similar analysis of the evolution of band structures for compressive and tensile strains, as shown in Figs. 4(b) and 4(d), shows that, for applied strains from -10% to 10%, a transition from direct to indirect semiconductor happens, while the transition from semiconductor to metal does not takes place in the strain region.

When applying strains along the bi direction from -10% to 10%, the changes in the band structures are more similar to those for strains along the a direction, and the transitions for both direct to indirect semiconductor and semiconductor to metal happen, as shown in Figs. 4(c) and 4(d), except that the latter transition occurs at a compressive strain of $\varepsilon_{xy} = -6\%$.

In addition, the evolution of band gaps in α-GeSe under various strains is shown in Fig. 4(d), indicating that the values of the calculated band gaps increase with the increase in tensile strains in the region from -10% to 10%, disregarding the directions along which the strains were applied.

Figure 5 shows the evolutions of band structures and values of the band gap of monolayer β-GeSe as a function of compressive and tensile strains with the strength from -10% to 10%. The behavior of β-GeSe under strain is quite different from that of α-GeSe. Monolayer β-GeSe without strain is an indirect semiconductor described by VBM V_X and CBM C_Y. When compressive strains are applied along the a direction, the values of V_X, C_X, and C_Y decrease, while V_S increases, leading to another type of indirect semiconductor. When applying a tensile strain along the a direction, the change in these VBMs and CBMs is contrary to the tendencies of compressive strain. We compared the evolutions of band structures under strain along the b and bi directions, as shown in Figs. 5(b) and 5(c), and came to the conclusion that the tendencies of V_X, C_X, and C_Y are similar to that along the a direction, but with large changes in V_S in the strain range from -10% to 10%. Furthermore, there is no transition from semiconductor to metal in this strain region.

It should be noted here that, although the band gap of monolayer β-GeSe decreases when the applied compressive strains increase, which is similar to the case of α-GeSe, the decreasing tendency of band gap when increasing tensile strains is opposite to that of α-GeSe. More interestingly, as shown in Figs. 5(b) and 5(d), for applied tensile strains along the b direction from 0% to 10%, both VBM (V_x) and CBM (C_x) locate along the Γ-X direction, and the values of VBM and CBM remain nearly unchanged, which means that the calculated band gaps subsequently remain nearly unchanged, around 1.73 eV. Such a robust band gap nearly independent of the tensile strains also leads to the near overlap of band gap curves for the two respective cases by applying tensile strains along the a and bi directions, as shown in Fig. 5(d).

As we know, that band gap is related to the bonding-antibonding splitting, which is determined quantitatively by the overlap integral V of atomic orbitals. The overlap integral V decreases with increasing interatomic distance, following the d^{-2} principle (d is the bond length) in covalent solids [52], i.e., $V \propto d^{-2}$. Thus, the energy width of each band increases when compressive strains are applied since the corresponding

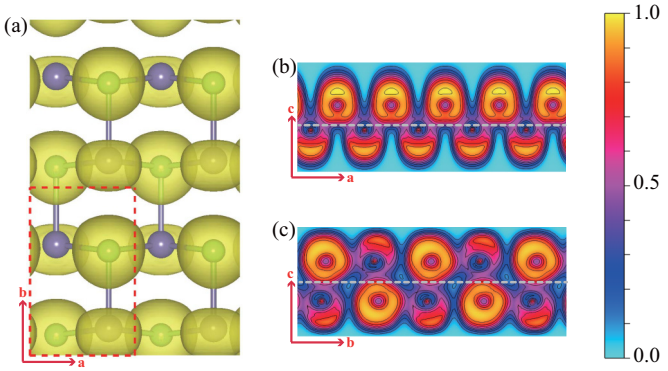

FIG. 6. (a) Top view of 3D ELF and 2D ELF profiles of monolayer β-GeSe along the (b) a and (c) b directions.

value of V increases due to a smaller d, as shown in Figs. 4(a) and 4(b) and 5(a) and 5(b). Similarly, when the tensile strains are applied, the band structure for covalent solids tends to become flat gradually due to the smaller value of V caused by a larger d. As shown in Table I and Fig. 1(d), monolayer β-GeSe has a relatively large bond length d_2 along the b direction. This means that the overlap integral along the b direction is smaller than that along the a direction, indicating that the change in band gap when applying tensile strains along the b direction will be much weaker.

To further understand the bond characteristics and then the mechanism of the robust band gap for monolayer β-GeSe, we have calculated the electronic localization function (ELF) [53–56], as shown in Fig. 6. The ELF is a position-dependent function with values that range from 0 to 1. ELF = 1 corresponds to perfect localization, and ELF = 0.5 corresponds to the electron-gas-like pair probability. The three-dimensional plot of the ELF in Fig. 6(a) shows that the covalent bond strength along the b direction is trivial compared with that along the a direction, which is reflected as well by the charge-density distribution for VBM and CBM shown in Fig. 3. Two-dimensional plots of ELF profiles in Figs. 6(b) and 6(c) show that electrons are localized on Se atom sites, and the Ge-Se bond strength along the b direction is weaker than that along the a direction. Therefore, when applying tensile strains along the b direction, the overlap integral will not fluctuate greatly due to the weak covalent bonds along the b direction, which may subsequently lead to the robust band gap insensitive to the tensile strains along the b direction, as shown in Fig. 5(d).

D. Transport properties of black phosphorene, monolayer α-MX, and β-GeSe

To investigate the transport properties of α- and β-GeSe, we systematically calculate carrier mobilities of black phosphorene, monolayer α-MX (α-GeS, α-GeSe, α-SnS, and α-SnSe), and β-GeSe. According to the deformation theory, i.e., Eq. (5), three parameters, namely, carrier effective mass m^*, the deformation potential E_l, and the elastic modulus C^{2D} in the propagation direction, determine the behaviors of carrier mobility of semiconductors [42,57]. Although the PBE calculations always underestimate the band gap, the curvatures of valence and conduction bands calculated using the PBE method are generally correct enough, and the calculated carrier mobilities are subsequently in good agreement with experiments for numerous 2D materials [40–42,57,58]. We calculate the effective masses of holes (m_h^*) and electrons (m_e^*) along the a and b directions by fitting parabolic functions to the band curve close to the VBM and CBM, respectively, as shown in Table II.

For black phosphorene, it is remarkable that along the a direction (band structure along the Γ-X direction in the Supplemental Material [46]), the valence of the band is nearly flat close to the Γ point (VBM), with an effective hole mass of $11.16m_0$, 9 times larger than the effective electron mass ($1.24m_0$). And along the b direction (Γ-Y direction in the band structure), the effective carrier masses are $0.14m_0$ (hole) and $0.15m_0$ (electron), respectively, mainly due to the more dispersive s and p characters of VBM and CBM, as shown in the band structure along the Γ-Y direction (see the Supplemental Material [46]).

As mentioned above, monolayer α-MX can be regarded as the phosphorene analogs produced by the so-called atomic

TABLE II. Calculated band gap E_g (HSE06 without SOC), effective mass m^* (with m_0^* being the static electron mass), deformation potential constant E_l, 2D elastic modulus C, and carrier mobility μ along the Γ-X and Γ-Y directions. The electron and hole carrier mobilities μ are calculated using Eq. (5) at $T = 300$ K.

Phase	E_g(HSE06) (eV)	Carrier type	m_a^* (units of m_0)	m_b^* (units of m_0)	E_{l-a} (eV)	E_{l-b} (eV)	C_a (N/m)	C_b (N/m)	μ_a (cm^2/V s)	μ_b (cm^2/V s)
Black phosphorene	1.49	hole	11.16	0.14	0.12	2.79	102.59	23.60	1.13×10^4	3.66×10^2
		electron	1.24	0.15	5.28	1.58	102.59	23.60	1.46×10^2	3.08×10^3
α-GeS	2.75	hole	0.87	0.25	4.57	6.45	42.36	12.89	1.06×10^2	5.70×10^1
		electron	0.46	0.23	3.24	0.47	42.36	12.89	5.73×10^2	1.69×10^4
α-GeSe	1.61	hole	0.33	0.16	9.67	5.20	37.00	14.00	1.10×10^2	3.10×10^2
		electron	0.27	0.15	6.83	1.45	37.00	14.00	3.07×10^2	4.71×10^3
α-SnS	1.50	hole	0.30	0.22	5.91	4.03	38.43	17.08	3.08×10^2	3.92×10^2
		electron	0.21	0.19	3.16	2.72	38.43	17.08	1.93×10^3	1.27×10^3
α-SnSe	0.98	hole	0.16	0.14	8.40	4.74	41.65	21.32	5.40×10^2	9.42×10^2
		electron	0.13	0.14	2.53	1.84	41.65	21.32	7.64×10^3	7.31×10^3
β-GeSe	2.47	hole	1.09	0.84	2.68	1.99	42.00	41.00	1.19×10^2	2.71×10^2
		electron	1.45	0.09	2.52	0.96	42.00	41.00	2.71×10^2	2.93×10^4

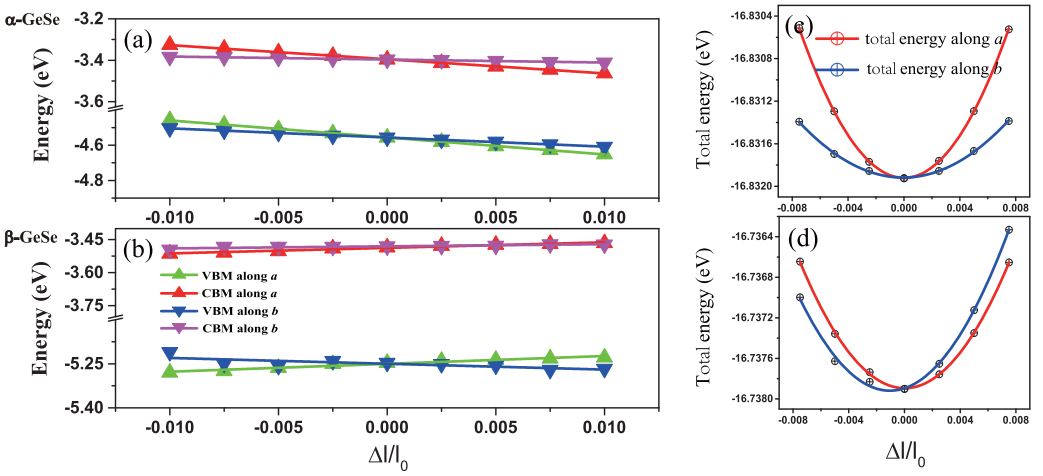

FIG. 7. Dependence of band edges with respect to vacuum as a function of applied uniaxial strains along the a and b directions for monolayer (a) α- and (b) β-GeSe. (c) and (d) The relationship between the total energy and strain along the a and b directions for α- and β-GeSe, respectively.

transmutation method; the band structures of the four monolayer α-MX compounds, i.e., α-GeS, α-GeSe, α-SnS, and α-SnSe, indeed show similar patterns, which are shown in Fig. 2(a) and the Supplemental Material [46]. All four monolayer α-MX compounds possess CBM along the Γ-X direction and VBM along the Γ-Y direction. According to the d^{-2} principle [52], the orbital overlapping integral V also determines the bandwidth of a specific band, and generally, a band with a larger bandwidth has a larger band curvature at the CBM/VBM points, which thus leads to smaller effective electron/hole masses for covalent solids. As shown in Table S1, the bond lengths $d_{1/2}$ for all the monolayer α-MX compounds have the tendency of $d_{\mathrm{GeS}} < d_{\mathrm{GeSe}} < d_{\mathrm{SnS}} < d_{\mathrm{SnSe}}$; therefore, the orbital overlapping V should be $V_{\mathrm{GeS}} > V_{\mathrm{GeSe}} > V_{\mathrm{SnS}} > V_{\mathrm{SnSe}}$ since the conduction and valence bands of all the monolayer α-MX compounds are formed by M p and X p orbitals, respectively. Subsequently, the effective masses for all the monolayer α-MX compounds can be ordered by $m^*_{\mathrm{GeS}} > m^*_{\mathrm{GeSe}} > m^*_{\mathrm{SnS}} > m^*_{\mathrm{SnSe}}$ due to the opposite tendency of the bandwidths for these four monolayer α-MX compounds. The relation of the effective masses for all the monolayer α-MX compounds is shown and confirmed in Table II as well.

By linearly fitting the band energy (CBM and VBM positions) shift with respect to the vacuum level under strain $\varepsilon(\Delta l/l_0)$ along the a and b directions, the DP constant E_l for both electrons and holes can be calculated. As shown in Figs. 7(a) and 7(b), the responses of CBM and VBM for α/β-GeSe to the applied strain appear to be anisotropic as well. The responses for black phosphorene, α-GeS, α-SnS, and α-SnSe are shown in the Supplemental Material [46]. The obtained DP constants E_l are listed in Table II.

The elastic constant C^{2D} can be calculated from the relation between the total energy and lattice dilations. Such relations for all the 2D materials under investigation here are shown in Figs. 7(c) and 7(d) and the Supplemental Material [46]. The calculated elastic constants are listed in Table II.

Based on the obtained m_e^*, E_l, and C^{2D}, the carrier mobilities of black phosphorene, monolayer α-MX (α-GeS, α-GeSe, α-SnS and α-SnSe), and β-GeSe at room temperature ($T = 300$ K) are calculated and listed in Table II. As shown in Table II, black phosphorene has a large hole carrier mobility of 1.13×10^4 cm^2/V s along the a direction, even with a large hole effective mass of $11.16m_0$, but with a large elastic modulus of 102.59 N/m, which is expected from the hybridized covalent sp^3 bonds and an extremely small band edge deformation potential constant of 0.12 eV, which can be understood by considering that for the band edge wave function the distribution of the electron state can have a significant impact on the lattice deformation [21]. Table II also shows the transport properties of monolayer α-MX, which show strongly anisotropic transport properties and high carrier mobilities along a and b directions.

The predicted carrier mobilities for both α- and β-GeSe are anisotropic along the a and b directions. Both α- and β-GeSe show high electron mobilities along the b direction μ_b, i.e., 4.71×10^3 cm^2/V s for monolayer α-GeSe and 2.93×10^4 cm^2/V s for monolayer β-GeSe. The calculated value of μ_b for β-GeSe is comparable to that of black phosphorene (1.13×10^4 cm^2/V s), which suggests that monolayer β-GeSe is also a promising candidate material for future electronic

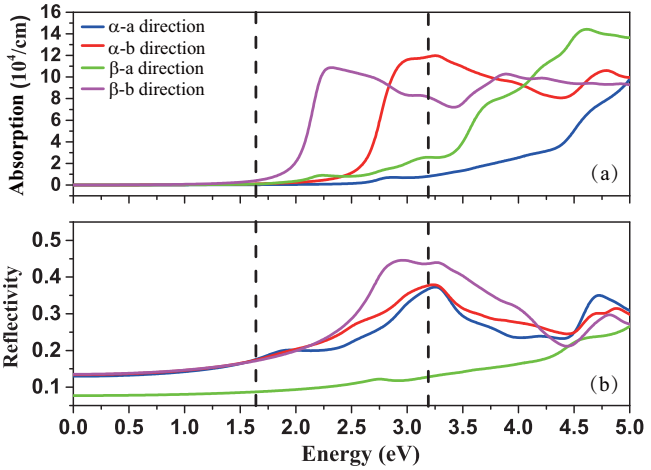

FIG. 8. HSE06 calculations of (a) optical absorption spectra and (b) the reflectivity of monolayer α- and β-GeSe for incident light with the polarization along the a and b directions.

and optoelectronic applications, considering the high electron mobilities and stability in an ordinary environment [27].

E. Optical properties of monolayer α- and β-GeSe

Figure 8 presents the in-plane optical absorption spectra $\alpha(\omega)$ and reflectivity $R(\omega)$ of monolayer α- and β-GeSe for the incident light with the polarization of the electric field **E** along the a (**E**//a) and b (**E**//b) directions, respectively. In 2D materials, compared to the band gap calculated using the quasiparticle GW method, which considers the excitonic effects, the optical band gap obtained with HSE06 is usually close to the real optical band gap due to the underestimation of band gap by neglecting excitonic effects [21]. Thus, we perform only HSE06 calculations of optical properties here. Further investigations of excitonic effects on electronic and optical properties of monolayer α- and β-GeSe are needed. The corresponding imaginary part of the dielectric function is shown in the Supplemental Material [46].

The absorption coefficient is defined as the decay of light intensity spreading in a unit length, i.e., Eq. (3). For monolayer α- and β-GeSe, the absorption coefficient shows an obvious anisotropy along different directions, and both materials exhibit obvious optical absorption with the frequency covering some part of the visible spectrum. The frequency region for high absorption along the b direction of β-GeSe is larger than that along the a direction shown in Fig. 8(a) and is even larger than those of α-GeSe irrespective of polarization directions. Such a significant anisotropic optical property can be used to identify the monolayer β-GeSe in experiments.

Figure 8(b) shows the reflectivity $R(\omega)$ for both monolayer α- and β-GeSe. The relatively less anisotropic property of α-GeSe and anisotropic property of β-GeSe are observed in the reflectivity curves, as shown in Fig. 8(b). For β-GeSe, $R(\omega)$ along the b direction in the visible region is higher than that of α-GeSe along both the a and b directions, which thus means that monolayer β-GeSe is a polarizationally nontransparent material.

IV. CONCLUSION

In summary, we have performed first-principles calculations on the structure, electronic, transport, and optical properties of monolayer α- and β-GeSe. α-GeSe is a puckered structure similar to that of black phosphorene with Ge and Se atoms substituted for P atoms alternately, while β-GeSe consists of six rings with the vertices arranged in an uncommon boat conformation. They all have strongly anisotropic properties. For monolayer α-GeSe, the direct-semiconducting characteristic is robust for small compression and moderate stretching along the b direction (from $\varepsilon_x = -1\%$ to $\varepsilon_x = 9\%$), and an extremely high electron mobility of 2.93×10^4 cm^2/V s for β-GeSe is observed along the armchair direction. Furthermore, the band gaps of monolayer β-GeSe remain nearly unchanged under tensile strain from 0% to 10%. The calculated optical properties of monolayer α- and β-GeSe show anisotropic behaviors and large absorption in some part of the visible spectrum. Due to the ultrahigh electron mobilities and the abnormal behavior of the robust band gap independent of the applied tensile strains, monolayer β-GeSe is promising for future electronic and optoelectronic applications.

ACKNOWLEDGMENTS

This work is supported by the National Natural Science Foundation of China under Grants No. 11374063 and No. 11404348 and the National Basic Research Program of China (973 Program) under Grant No. 2013CBA01505. Work at Ames Laboratory is partially supported by the U.S. Department of Energy, Office of Basic Energy Science, Division of Materials Science and Engineering (Ames Laboratory is operated for the U.S. Department of Energy by Iowa State University under Contract No. DE-AC02-07CH11358). The European Research Council under ERC Advanced Grant No. 320081 (PHOTOMETA) supports work at FORTH.

[1] K. S. Novoselov, A. K. Geim, S. V. Morozov, D. Jiang, Y. Zhang, S. V. Dubonos, I. V. Grigorieva, and A. A. Firsov, Electric field effect in atomically thin carbon films, Science **306**, 666 (2004).

[2] K. S. Novoselov, A. K. Geim, S. V. Morozov, D. Jiang, M. I. Katsnelson, I. V. Grigorieva, A. A. Dubonos, and S. V. Firsov, Two-dimensional gas of massless Dirac fermions in graphene, Nature (London) **438**, 197 (2005).

[3] Y. B. Zhang, Y. W. Tan, H. L. Stormer and P. Kim, Experimental observation of the quantum Hall effect and Berry's phase in graphene, Nature (London) **438**, 201 (2005).

[4] A. A. Balandin, Thermal properties of graphene and nanostructured carbon materials, Nat. Mater. **10**, 569 (2011).

[5] A. A. Balandin, S. Ghosh, W. Z. Bao, I. Calizo, D. Teweldebrhan, F. Miao, and C. N. Lau, Superior thermal conductivity of single-layer graphene, Nano Lett. **8**, 902 (2008).

[6] F. Schedin, A. K. Geim, S. V. Morozov, E. W. Hill, P. Blake, M. I. Katsnelson, and K. S. Novoselov, Detection of individual gas molecules adsorbed on graphene, Nat. Mater. **6**, 652 (2007).

[7] K. Kaasbjerg, K. S. Thygesen, and K. W. Jacobsen, Phonon-limited mobility in n-type single-layer MoS_2 from first principles, Phys. Rev. B **85**, 115317 (2012).

[8] H. J. Conley, B. Wang, J. I. Ziegler, Jr., R. F. Haglund, S. T. Pantelides, and K. I. Bolotin, Bandgap engineering of strained monolayer and bilayer MoS_2, Nano Lett. **13**, 3626 (2013).

[9] W. S. Yun, S. W. Han, S. C. Hong, I. G. Kim, and J. D. Lee, Thickness and strain effects on electronic structures of transition metal dichalcogenides: 2H-MX_2 semiconductors (M = Mo, W; X = S, Se, Te), Phys. Rev. B **85**, 033305 (2012).

[10] A. Kumar and P. K. Ahluwalia, Electronic structure of transition metal dichalcogenides monolayers 1H-MX_2 (M = Mo, W; X = S, Se, Te) from ab-initio theory: New direct band gap semiconductors, Eur. Phy. J. B **85**, 186 (2012).

[11] F. F. Zhu, W. J. Chen, Y. Xu, C. L. Gao, D. D. Guan, C. H. Liu, D. Qian, S. C. Zhang, and J. F. Jia, Epitaxial growth of two-dimensional stanene, Nat. Mater. **14**, 1020 (2015).

[12] S. Balendhran, S. Walia, H. Nili, S. Sriram, and M. Bhaskaran, Elemental analogues of graphene: Silicene, germanene, stanene, and phosphorene, Small **11**, 640 (2015).
[13] S. H Zhang, J. Zhou, Q. Wang, X. S. Chen, Y. Kawazoe, and P. Jena, Penta-graphene: A new carbon allotrope, Proc. Natl. Acad. Sci. U.S.A. **112**, 2372 (2015).
[14] Y. F. Xu, Z. Y. Ning, H. Zhang, G. Ni, H. Z. Shao, B. Peng, X. C. Zhang, X. Y. He, Y. Y. Zhu, and H. Y. Zhu, Anisotropic ultrahigh hole mobility in two-dimensional penta-SiC_2 by strain-engineering: Electronic structure and chemical bonding analysis, RSC Adv. **7**, 45705 (2017).
[15] J. S. Qiao, X. H. Kong, Z.-X. Hu, F. Yang, and W. Ji, High-mobility transport anisotropy and linear dichroism in few-layer black phosphorus, Nat. Commun. **5**, 4475 (2014).
[16] T. Hong, B. Chamlagain, W. Z. Lin, H. J. Chuang, M. Pan, Z. X. Zhou, and Y. Q. Xu, Polarized photocurrent response in black phosphorus field-effect transistors, Nanoscale **6**, 8978 (2014).
[17] H. Liu, A. T. Neal, Z. Zhu, Z. Luo, X. F. Xu, D. Tomaének, and P. D. Ye, Phosphorene: An unexplored 2D semiconductor with a high hole mobility, Acs. Nano. **8**, 4033 (2014).
[18] J. Liu, G. M. Choi, and D. G. Cahill, Measurement of the anisotropic thermal conductivity of molybdenum disulfide by the time-resolved magneto-optic Kerr effect, J. Appl. Phys. **116**, 233107 (2014).
[19] V. Eswaraiah, Q. S. Zeng, Y. Long, and Z. Liu, Black phosphorus nanosheets: Synthesis, characterization and applications, Small **12**, 3480 (2016).
[20] L. C. Gomes and A. Carvalho, Phosphorene analogues: Isoelectronic two-dimensional group-IV monochalcogenides with orthorhombic structure, Phys. Rev. B **92**, 085406 (2015).
[21] J. H. Yang, Y. Y. Zhang, W. J. Yin, X. G. Gong, B. I. Yakobson, and S. H. Wei, Two-dimensional SiS layers with promising electronic and optoelectronic properties: Theoretical prediction, Nano Lett. **16**, 1110 (2016).
[22] Y. G. Zhou, MX (M = Ge, Sn; X = S, Se) sheets: Theoretical prediction of new promising electrode materials for Li ion batteries, J. Mater. Chem. **4**, 10906 (2016).
[23] H. Wang and X. F. Qian, Two-dimensional multiferroics in monolayer group IV monochalcogenides, 2D Mater. **4**, 015042 (2017).
[24] R. X. Fei, W. B. Li, J. Li, and L. Yang, Giant piezoelectricity of monolayer group IV monochalcogenides: SnSe, SnS, GeSe, and GeS, Appl. Phys. Lett. **107**, 173104 (2015).
[25] A. Shafique and Y. H. Shin, Thermoelectric and phonon transport properties of two-dimensional IV-VI compounds, Sci. Rep. **7**, 506 (2017).
[26] L. D. Zhao, S. H. Lo, Y. S. Zhang, H. Sun, G. J. Tan, C. Uher, C. Wolverton, V. P. Dravid, and M. G. Kanatzidis, Ultralow thermal conductivity and high thermoelectric figure of merit in SnSe crystals, Nature (London) **508**, 373 (2014).
[27] F. O. von Rohr, H. W. Ji, F. A. Cevallos, T. Gao, N. P. Ong, and R. J. Cava, High-pressure synthesis and characterization of β-GeSe—A six-membered-ring semiconductor in an uncommon boat conformation, J. Am. Chem. Soc. **139**, 2771 (2017).
[28] H. Wiedemeier von Schnering and H. Georg, Refinement of the structures of GeS, GeSe, SnS and SnSe, Z. Kristallogr. Cryst. Mater. **148**, 295 (1978).
[29] G. Kresse and J. Furthmüller, Efficient iterative schemes for *ab initio* total-energy calculations using a plane-wave basis set, Phys. Rev. B **54**, 11169 (1996).
[30] J. Heyd, G. E. Scuseria, and M. Ernzerhof, Hybrid functionals based on a screened Coulomb potential, J. Chem. Phys. **118**, 8207 (2003); Erratum: "Hybrid functionals based on a screened Coulomb potential" [J. Chem. Phys. 118, 8207 (2003)] **124**, 219906 (2006).
[31] J. P. Perdew, K. Burke, and M. Ernzerhof, Generalized Gradient Approximation Made Simple, Phys. Rev. Lett. **77**, 3865 (1996).
[32] S. Grimme, Semiempirical GGA-type density functional constructed with a long-range dispersion correction, J. Comput. Chem. **27**, 1787 (2006).
[33] M. Gajdoš, K. Hummer, G. Kresse, J. Fürthmuller, and F. Bechstedt, Linear optical properties in the projector-augmented wave methodology, Phys. Rev. B **73**, 045112 (2006).
[34] M. S. Dresselhaus, *Solid State Physics Part II-Optical Properties of Solids*, Lecture Notes Part 2 (2001), http://web.mit.edu/course/6/6.732/www/6.732-pt2.pdf.
[35] S. Saha, T. P. Sinha, and A. Mookerjee, Electronic structure, chemical bonding, and optical properties of paraelectric $BaTiO_3$, Phys. Rev. B **62**, 8828 (2000).
[36] B. C. Luo, X. H. Wang, E. Tian, G. W. Li, and L. T. Li, Electronic structure, optical and dielectric properties of $BaTiO_3/CaTiO_3/SrTiO_3$ ferroelectric superlattices from first-principles calculations, J. Mater. Chem. C **3**, 8625 (2015).
[37] Y. F. Xu, B. Peng, H. Zhang, H. Z. Shao, R. J. Zhang, and H. Y. Zhu, First-principle calculations of optical properties of monolayer arsenene and antimonene allotropes, Ann. Phys. (Berlin) **529**, 1600152 (2017).
[38] J. Bardeen and W. Shockley, Deformation potentials and mobilities in non-polar crystals, Phys. Rev. **80**, 72 (1950).
[39] Y. Nakamura, T. Q. Zhao, J. Y. Xi, W. Shi, D. Wang, and Z. G. Shuai, Intrinsic charge transport in stanene: Roles of bucklings and electron-phonon couplings, Adv. Electron. Mater. **3**, 1700143 (2017).
[40] Y. Cai, G. Zhang, and Y. W. Zhang, Polarity-reversed robust carrier mobility in monolayer MoS_2 nanoribbons, J. Am. Chem. Soc. **136**, 6269 (2014).
[41] M. Q. Long, L. Tang, D. Wang, Y. L. Li, and Z. G. Shuai, Electronic structure and carrier mobility in graphdiyne sheet and nanoribbons: Theoretical predictions, ACS Nano. **5**, 2593 (2011).
[42] J. M. Chen, J. Y. Xi, D. Wang, and Z. G. Shuai, Carrier mobility in graphyne should be even larger than that in graphene: A theoretical prediction, J. Phys. Chem. Lett. **4**, 1443 (2013).
[43] Y. L. Wang and Y. Ding, Electronic structure and carrier mobilities of arsenene and antimonene nanoribbons: A first-principle study, Nanoscale Res. Lett. **10**, 254 (2015).
[44] F. Li, X. H. Liu, Y. Wang, and Y. F. Li, Germanium monosulfide monolayer: A novel two-dimensional semiconductor with a high carrier mobility, J. Mater. Chem. C **4**, 2155 (2016).
[45] R. X. Fei and L. Yang, Strain-engineering the anisotropic electrical conductance of few-layer black phosphorus, Nano Lett. **14**, 2884 (2014).
[46] See Supplemental Material at http://link.aps.org/supplemental/10.1103/PhysRevB.96.245421 for details of data analysis.

[47] Y. D. Hu, S. L. Zhang, S. F. Sun, M. Q. Xie, B. Cai, and H. B. Zeng, GeSe monolayer semiconductor with tunable direct band gap and small carrier effective mass, Appl. Phys. Lett. **107**, 122107 (2015).

[48] M. H. Wu and X. C. Zeng, Intrinsic ferroelasticity and/or multiferroicity in two-dimensional phosphorene and phosphorene analogues, Nano Lett. **16**, 3236 (2016).

[49] A. K. Singh and R. G. Hennig, Computational prediction of two-dimensional group-IV mono-chalcogenides, Appl. Phys. Lett. **105**, 042103 (2014).

[50] C. Si, Z. M. Sun, and F. Liu, Strain engineering of graphene: A review, Nanoscale **8**, 3207 (2016).

[51] R. Qin, C. H. Wang, W. J. Zhu, and Y. L. Zhang, First-principles calculations of mechanical and electronic properties of silicene under strain, AIP Adv. **2**, 022159 (2012).

[52] Y. K. Sun, S. E. Thompson, and T. Nishida, *Strain Effect in Semiconductors* (Springer, Berlin, 2010).

[53] A. D. Becke and K. E. Edgecombe, A simple measure of electron localization in atomic and molecular systems, J. Chem. Phys. **92**, 5397 (1990).

[54] A. Savin, O. Jepsen, J. Flad, O. K. Andersen, H. Preuss, and H. G. von Schnering, Electron localization in solid-state structures of the elements: The diamond structure, Angew. Chem., Int. Ed. Engl. **31**, 187 (1992).

[55] C. Gatti, Chemical bonding in crystals: New directions, Z. Kristallogr. Cryst. Mater. **220**, 399 (2005).

[56] K. Chen and S. Kamran, Bonding characteristics of TiC and tin, Model. Numer. Simul. Mater. Sci. **3**, 7 (2013).

[57] J. Y. Xi, M. Q. Long, L. Tang, D. Wang, and Z. G. Shuai, First-principles prediction of charge mobility in carbon and organic nanomaterials, Nanoscale **4**, 4348 (2012).

[58] J. Dai and X. C. Zeng, Titanium trisulfide monolayer: Theoretical prediction of a new direct-gap semiconductor with high and anisotropic carrier mobility, Angew. Chem. **127**, 7682 (2015).